Chapter 10
Fiber-Optical 3D Shape Sensing

Christian Waltermann, Jan Koch, Martin Angelmahr, Jörg Burgmeier, Markus Thiel, and Wolfgang Schade

10.1 Introduction

Fiber Bragg grating (FBG) technology is well known since more than three decades. It started in 1978 with the discovery of photosensitivity in optical fibers by Ken Hill et al. [1] when illuminating germanium-doped silica fibers with visible argon ion laser radiation. In this context, first periodic refractive index variation was introduced into the core of such special optical fibers. However, for nearly one decade, there was found no real application of these fundamental observations. The major breakthrough for Bragg gratings came in 1988 with the report on holographic writing applying single-photon absorption in the ultraviolet by Metz et al. [2]. They demonstrated reflection gratings using two interfering laser beams imaged into the fiber core. This was the starting point for several applications of FBGs ranging from reflection gratings used in telecommunication, high reflectivity end reflectors in fiber lasers, or sensor applications for monitoring mechanical strain and temperature.

In 2004 FBG technology became a new strong impact by the first demonstration of direct point-by-point writing of FBGs applying femtosecond laser pulses [3, 4]. Advantages compared to conventional methods such as phase mask or interferometric processing are an improved mechanical stability of the fiber in the area where the FBG is processed, a fiber core diameter of typically 9 µm for wavelengths around 1,500 nm, and a maximum of flexibility while processing the FBG because the

C. Waltermann • J. Koch • M. Angelmahr • J. Burgmeier • M. Thiel
Fraunhofer Heinrich-Hertz-Institut (HHI), EnergieCampus,
Am Stollen 19B, 38640 Goslar, Germany

W. Schade (✉)
Institut für Energieforschung und Physikalische Technologien (IEPT),
Energie-Forschungszentrum Niedersachsen (EFZN), Technische Universität Clausthal,
Am Stollen 19B, 38640 Goslar, Germany

Fraunhofer Heinrich-Hertz-Institut (HHI), EnergieCampus, Am Stollen 19B, 38640 Goslar,
Germany
e-mail: wolfgang.schade@tu-clausthal.de

only limitation for the direct point-by-point writing of periodic index modulation in optical fibers is the optical transparency of the cladding. Recent results show that applying femtosecond laser for point-by-point writing can achieve single FBGs with reflectivity ranging from 10^{-4} up to nearly 100 % just by changing the laser parameters and adapting the number of grating points, FBG arrays of up to 20 gratings with nearly equal reflectivity and side-band suppression down to 20 dB, or even π-shifted FBGs with bandwidths less than 3 pm, just to mention some examples.

Besides this, very recent results have shown that using the femtosecond laser technology, optical waveguides, and FBGs can directly be written not only into the bulk material of a glass sample but also into the cladding of an optical fiber. This means the processing of photonic structures is not limited any more only to the fiber core and offers completely new possibilities for 3-dimensional (3D) shape measurements of mechanical devices applying optical fibers and FBG sensors. Up to now a combination of three optical fibers with integrated FBG sensors or the use of multicore fibers with FBGs has been used for 3D shape measurements [5, 6] with the disadvantage that mechanical flexibility is limited when, for example, three fibers have to be integrated into a medical catheter for shape measurement. In addition, multicore fibers need special optics for individual readout of the Bragg signals from the single cores. Direct femtosecond laser-based processing of FBGs into the core and the cladding of an optical fiber make it possible using just a single standard one-core optical fiber for 3D shape monitoring with the advantages of no need for additional optics, the high mechanical flexibility of a single 125 or 80 μm fiber, and the use of commercially available standard fiber connectors and components that are well known from telecommunication.

In this chapter a summary of the state of the art for femtosecond laser direct writing of FBGs with special view to applications in 3D shape monitoring for medical applications is given. These very new results are not only limited to medical but will also find interesting applications in oil and gas industry, e.g., for monitoring and long-term inspection of bore holes and drilling wells.

10.2 Femtosecond Laser Processing of FBGs

10.2.1 Theory of FBGs

FBG can be described as periodical variation of the refractive index along the fiber core. For a cosine modulation, the refractive index can be written as

$$n(x) = n_0 + \Delta n \cos\left(\frac{2\pi z}{\Lambda}\right) \tag{10.1}$$

where n_0 represents the average refractive index of the fiber core, Δn *is* the variation of the refractive index (typically 10^{-5}–10^{-2}) [7], Λ is the grating constant, and z is
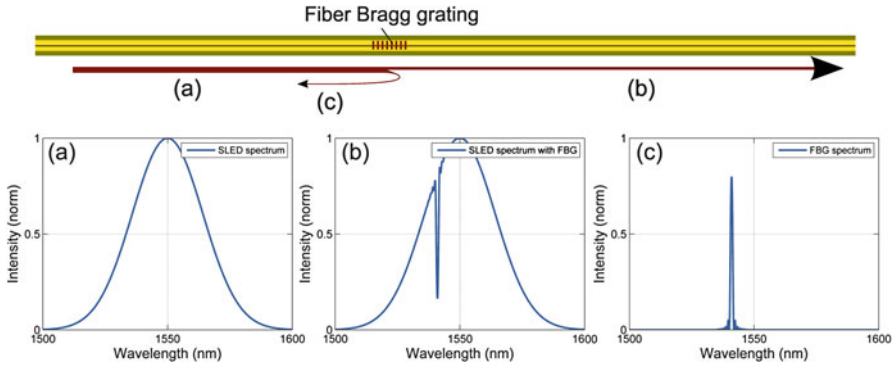
Fig. 10.1 Basic principle of fiber Bragg grating sensor interrogation. Spectral broadband light (**a**) is guided through an optical fiber. Light that fits the Bragg condition is missing in the transmitted spectrum (**b**) and occurs as reflection peak (**c**)

the position along the fiber, respectively. This periodic index modulation reflects certain light components which fit the so-called Bragg condition:

$$m\lambda_B = 2n_{eff}\,\Lambda \text{ with } m = (1, 2, 3, \dots) \tag{10.2}$$

where λ_B is the center wavelength of the back-reflected light and n_{eff} is the effective refractive index of the fiber core material including the periodic modulation of the refractive index. Therefore, an FBG can be described as a spectral filter element as shown in Fig. 10.1.

Applying the coupled-mode theory with the assumption of a constant modulation amplitude and periodicity, the following expression concerning the reflection properties of FBGs is obtained [7]:

$$R(L, \lambda) = \frac{\kappa^2 \sinh^2(sL)}{\Delta k^2 \sinh^2(sL) + s^2 \cosh^2(sL)} \tag{10.3}$$

where $R(L, \lambda)$ is the reflectivity, which depends on the grating length L and the wavelength λ, κ is the coupling coefficient, Δk is the detuning wave vector given by $\Delta k = 2\pi n_{eff}/\lambda - \pi/\lambda$, and, finally, $s = \sqrt{\kappa^2 - \Delta k^2}$. For a sinusoidal modulation of the refractive index, the coupling coefficient κ is determined by

$$\kappa = \frac{\pi\,\Delta n\,\eta(V)}{\lambda} \text{ with } \eta(V) \approx 1 - \frac{1}{V^2} \tag{10.4}$$

where η is a function of the fiber parameter V ($V \geq 2.4$) [7] representing the fraction of the integrated fundamental mode intensity within the core (Δn is the change of refractive index). At the FBG center wavelength, Δk is zero and the equation of reflectivity can be simplified to

Fig. 10.2 Simulated reflection spectrum of a fiber Bragg grating with a constant coupling coefficient ($\kappa = 0.52$ 1/mm; $L = 1.9$ mm; $\Delta n = 1.8 \times 10^{-4}$)
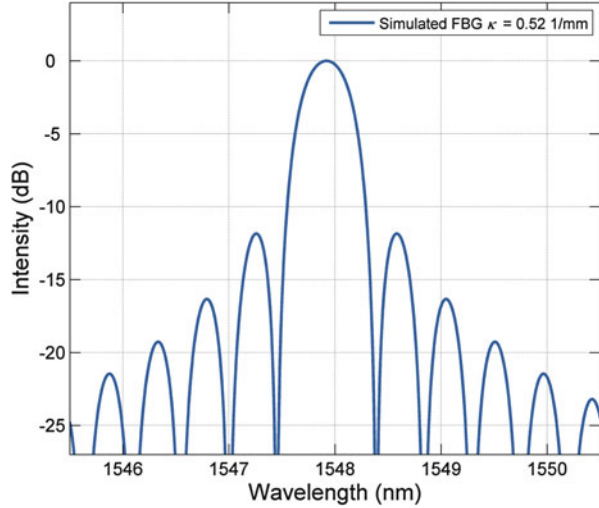
$$R(L, \lambda) = \tanh^2(\kappa L) \qquad (10.5)$$

Based on this equation it can be identified that the reflectivity will increase if the change of refractive index or the length of the grating increases (Fig. 10.2).

The second important property of FBGs is the reflection bandwidth. A general expression for the approximation of the full width at first zeros (FWFZ) bandwidth for a first-order grating is given by [8]

$$\Delta\lambda_{FWFZ} = \frac{\lambda^2}{\pi n_{eff} L} \sqrt{(\kappa L)^2 + \pi^2} \qquad (10.6)$$

In the case of weak coupling ($\kappa L < 1$), this equation can be simplified to

$$\Delta\lambda_{FWFZ} = \frac{\lambda^2}{n_{eff} L} \qquad (10.7)$$

Consequently, the bandwidth for weak gratings is inversely proportional to the grating length L and is very narrow for very long FBGs, whereas, in the case of strong coupling ($\kappa L \gg 1$), the bandwidth can be approximated by

$$\Delta\lambda_{FWFZ} = \frac{\lambda^2 \gg}{\pi n_{eff}} \qquad (10.8)$$

Here, the bandwidth is directly proportional to the coupling coefficient κ. However, the bandwidth of FBGs may be additionally influenced by other parameters leading to special kinds of FBGs such as so-called chirped, apodized, or phase-shifted gratings. These types of gratings will be discussed more in detail in Sect. 10.2.3.

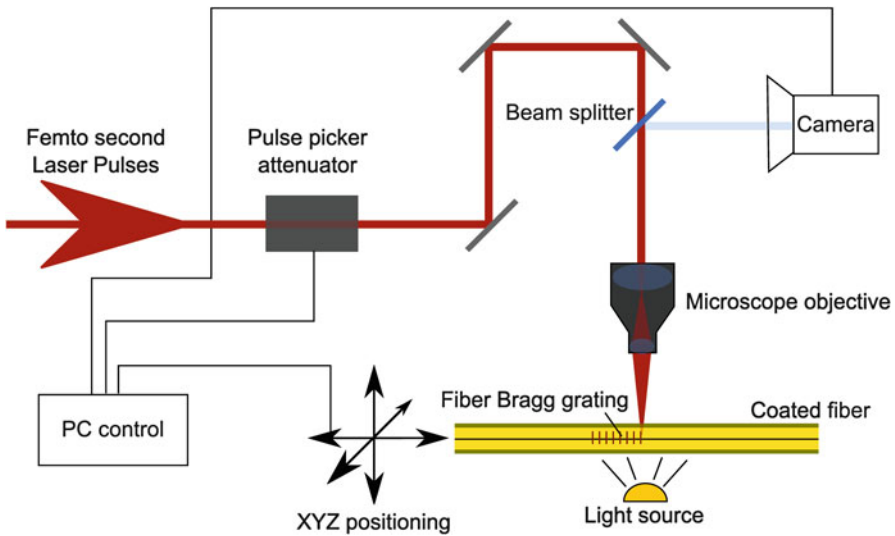## 10.2.2 Point-by-Point FBG Fabrication by Femtosecond Laser Pulses

Since the first realization of FBGs by Hill in 1978 [1], several different manufacturing processes were described. To date, one of the main manufacturing methods is based on the irradiation of photosensitive, typically germanium-doped optical fibers with an intense ultraviolet source (such as an ultraviolet excimer laser). The variation of refractive index within the fiber core is achieved by two-beam laser interference or a photomask. With these methods, FBGs can be produced in sufficiently high quality. Typically this is done during the fabrication process of the fiber in the draw tower. Otherwise special, photosensitive, and uncoated optical fibers have to be provided. Taking these disadvantages into account, a rather new production method was firstly demonstrated in 2004: the point-by-point inscription of FBGs applying femtosecond laser technology [3, 9]. With this method, doped and, most importantly, undoped standard optical fibers can be used for direct FBG fabrication. In addition, the inscription process is possible without any problem directly through the fiber coating unless the coating material is optically transparent for the wavelength of the laser used for processing (typically 800 nm). For example, acrylate, polyimide, and Ormocer® coatings are sufficiently optical transparent for laser radiation around 800 nm [10]. Finally, the point-by-point inscription enables the adjustment of nearby every preferred FBG parameter without the modification of the writing setup and therefore the complete spectrum of customized FBGs can easily be processed by using standard optical fibers [11].

For undoped quartz glass, the band gap is determined to be 9 eV [12] but is only optically transparent for light $\lambda \geq 200$ nm ($\sim$6 eV). Therefore, only for doped fibers with a smaller band gap, photomask FBG inscription techniques can be applied. However, for an extreme high energy densities ($>10^{10}$ W/cm^2), multiphoton processes will be initiated within the bulk glass material. Within a femtosecond laser focus, such high energy densities can be obtained and a nonlinear light material interaction occurs. Electrons in the so-called valence band can be lifted into the conduction band by the multiphoton absorption as shown in Fig. 10.3. As a consequence, the absorbed energy leads to a local variation of the refractive index. The probability of these processes increases exponentially with the amount of required photons. Furthermore, electrons can reach the conduction band due to the tunnel effect even if not enough photons are resent that are required for the multiphoton processes.

The setup for the point-by-point inscription of FBG applying a femtosecond laser is presented in Fig. 10.4. A regenerative ultrashort pulse laser amplifier generates light pulses with 100 femtosecond pulse duration, repetition rate in the kilohertz range, and a single-pulse energy of >1 mJ. However, only about 0.3 μJ are necessary for the FBG processing. The laser beam is focused into the center of the fiber core using a microscope objective. If the fiber core is moved with constant speed along its optical axis while illuminating with laser pulses of constant repetition rate (e.g., 100 Hz), the induced variation of the refractive index will be periodic and an FBG
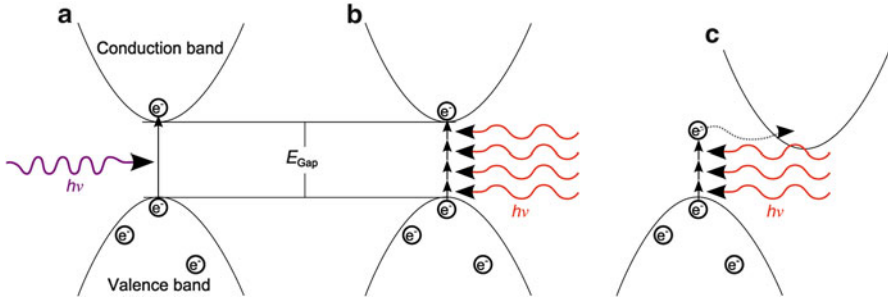
Fig. 10.3 Possible absorption processes: (**a**) regular photon absorption, (**b**) multiphoton absorption, and (**c**) multiphoton absorption and tunnel ionization

Fig. 10.4 Setup for the point-by-point fiber Bragg grating inscription by femtosecond laser pulses

will be generated. Applying an external pulse picker and light attenuator, the exact pulse specification can be adjusted for any required customization. The laser pulse specifications can be adjusted prior or even adapted during the inscribing process using a genetic algorithm.

By application of a smart combination of various different inscription parameters, like grating order, pulse energy, or special gate drive of the pulse picker, nearly every type of FBG mentioned in the literature can be processed without any fundamental change of the setup. Some examples of customized FBGs will be discussed in the following.
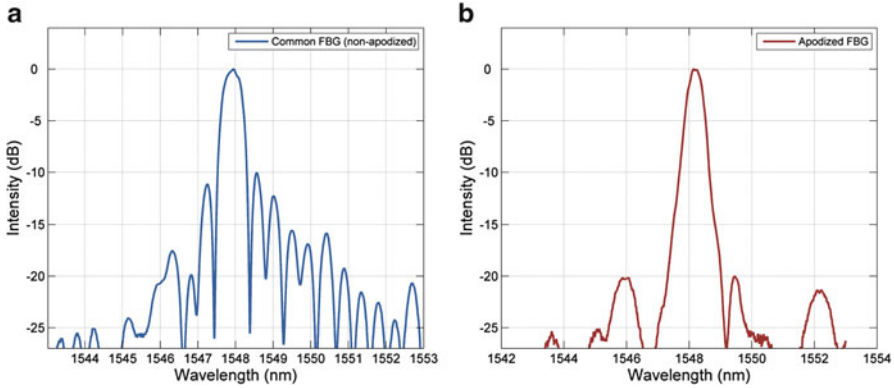
Fig. 10.5 (**a**) Normalized spectrum of a common Bragg reflector inscribed point-by-point with a femtosecond laser. (**b**) Apodized grating with a side-band suppression of −20 dB

10.2.3 Types of FBGs

The simplest FBG is called common Bragg reflector [13]. Such a grating has a constant coupling and grating constant as well as a sinusoidal change of the refractive index. According to the coupled-mode theory and Eq. (10.3), the reflective spectra of such grating depend mainly on the grating length L, the coupling constant κ, and the effective refractive index n_{eff} of the material. A typical normalized reflective spectrum of a common Bragg grating with a length of $L = 2$ mm and a refractive index variation of $\Delta n = 1.8 \times 10^{-4}$ inscribed through a polyimide-coated optical fiber applying point-by-point femtosecond laser technique is shown in Fig. 10.5.

However, even for a perfect common grating, the slopes of the main reflection peak will show side lobes with a peak reflectivity of approximately 10 dB. For some data analysis algorithms applied in sensor applications of FBGs these side lobes can lead to detection errors and uncertainties. A Gaussian intensity modulation of the induced periodic refractive index change in the fiber core reduces the peak intensity of side loops significantly [14]. For photomask-inscribed gratings a side lobe suppression of up to −30 dB is demonstrated [15]. These so-called apodized gratings are often used as sharp band filters in dense-wavelength-division-multiplexing (DWDM) applications [13]. Figure 10.5b shows an apodized FBG inscribed with the same femtosecond laser parameters as used for the grating in (a) but writing the grating diagonal with respect to the center line of the fiber core. Then the side lobes of the reflective spectrum are one order of magnitude smaller and the main peak resembles a Gaussian shape. In this configuration a side-band suppression of more than −20 dB is obtained.

Furthermore, the point-by-point femtosecond laser processing technology allows that FBGs may be aligned in customized arrays without the requirement of any splices. Distances between single FBGs can range from micrometers up to several meters and more. The reflection spectrum of such a customized fiber-optical Bragg
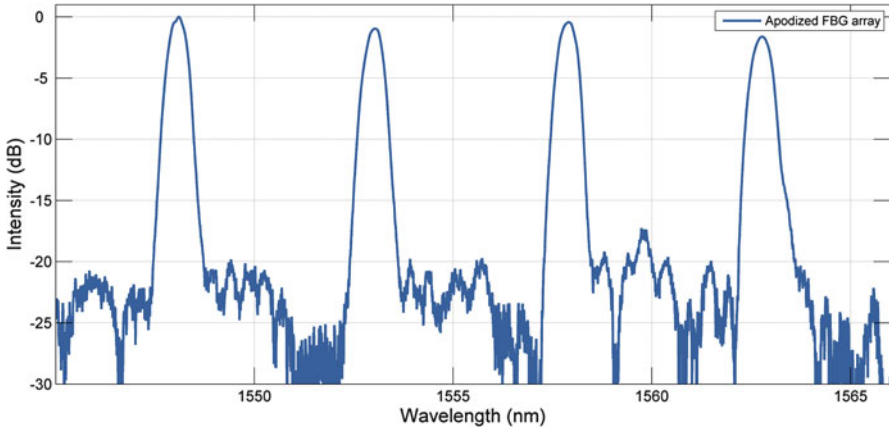
Fig. 10.6 Array of four apodized fiber Bragg gratings

grating array is shown in Fig. 10.6. The equal light intensity reflection and side lobe suppression of each grating result in an easy readout by commercially available interrogation units.

Most conventionally processed FBG sensors require a doping of the fiber which results in a reduced core diameter of 6 μm because the mode field diameter has to be adopted for single-mode light guiding at 1,550 nm. Typical undoped telecom fibers for 1,550 nm have a diameter of 9 μm. This difference in core diameter results in significant losses when combining several conventionally processed FBGs with patch cables. For the spectrum shown in Fig. 10.6, four FBGs each with 0.5 nm bandwidth were processed with an equidistant spacing of 100.0 cm in a polyimide-coated optical fiber. Arrays of more than 20 high reflective FBGs have been fabricated by the point-by-point femtosecond laser technology.

Depending on the chosen parameters, FBGs with nearly arbitrary reflectivities and bandwidths can be processed. Typical gratings have a reflectivity R between 0.0001 % and >90 %. The full width at half maximum can be adjusted between approximately 50 pm for high-order long gratings and several nanometers for short gratings ($L < 1$ mm) written in first-order mode. Figure 10.7a shows a common Bragg reflector with a reflectivity about 10 % and a full width at half maximum of 5.0 nm.

For high accuracy measurements, very narrowband FBGs are required. This specification is obtained by processing phase-shifted or so-called π-shifted FBGs. In this case, two high reflective gratings are processed direct behind each other phase shifted with half of their wavelength [13, 16, 17]. Interference between the two gratings leads to a very narrow transmission peak at the spectral center wavelength. The transmission spectrum of such a π-shifted FBG is shown in Fig. 10.7b. The spectral bandwidth is <5.0 pm.

Due to the small spatial size of each single grating dot (down to less than one cubic micrometer—determined by the focal diameter of the laser spot and even more
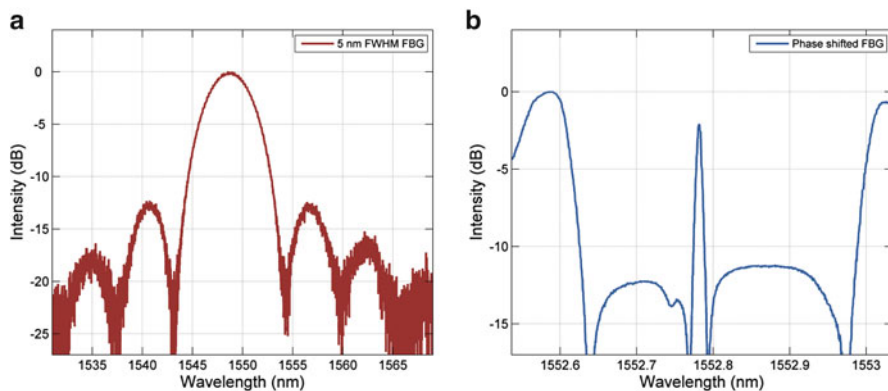
Fig. 10.7 (**a**) Reflected spectrum of a short first-order fiber Bragg grating. (**b**) Transmission spectrum of π-shifted fiber Bragg grating

reduced by the nonlinear multiphoton absorption process) when using the point-by-point femtosecond laser technology for fabrication of FBGs, spatially separated FBGs can be processed in the single core of a multicore fiber and even superimposed within a single-mode fiber core.

10.2.4 Processing with Shaped Femtosecond Pulses

The femtosecond laser processing of FBGs in optical fibers may lead to local damage of the glass which in consequence will result in reduced mechanical stability of the fiber and therefore such gratings cannot be used for applications where high mechanical stress of the fiber (elongation >3 %) is required. In this context the processing of FBGs with shaped femtosecond pulses—here pulse trains instead of a single Gaussian pulse intensity profile are discussed—will lead to significantly reduced modification of the fiber material and therefore to much higher mechanical stability. One example is shown in Fig. 10.8. In (a) the single-pulse and the multi-pulse excitation scheme is schematically shown. Conventionally a single femtosecond laser pulse creates an index change and the Bragg grating is the sum of n individual laser pulses. In the case of pulse shaping, each Bragg grating point is generated by a train of femtosecond laser pulses. Using 20 laser pulses and a pulse energy of 280 nJ for processing, a grating point results in an index change of $\Delta n = 1.4 \times 10^{-3}$ while a single pulse with much higher pulse energy of 470 nJ only gives an index change of $\Delta n = 8.4 \times 10^{-4}$. This also results in a change of the transmission intensity as shown in part (b) of the figure. These first results show that femtosecond pulse train FBG processing is preferred compared to single-shot methods due to significantly reduced pulse energy and therefore less damage of the glass material.
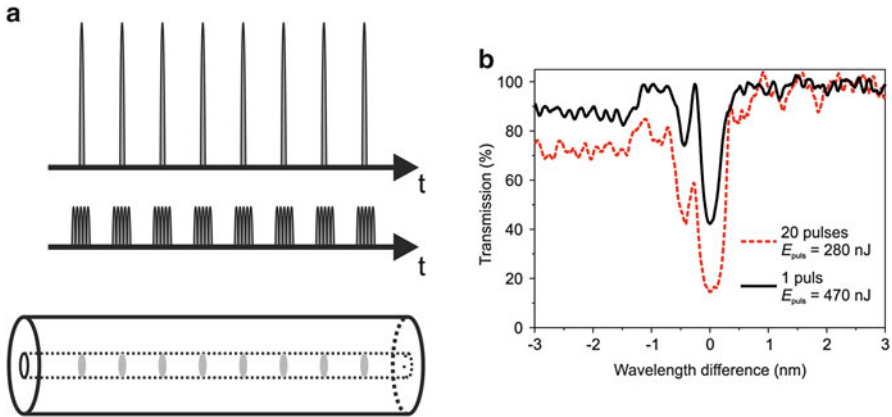
Fig. 10.8 (**a**) Single-shot and shaped (pulse train) FBG processing. (**b**) Transmission of an FBG processed by single femtosecond laser pulses (*solid line*) and a pulse train (*dashed line*) consisting of 20 individual pulses

10.3 Fiber-Optical 3D Shape Sensor Technology

10.3.1 Optical Multiplexing

One of the major advantages of FBGs compared to conventional electrical strain gauges is the possibility of simple sensor multiplexing [18]. One conventional strain gauge needs at least two electrical cables; however, hundreds of FBGs can be processed directly into one optical fiber at different local positions and these FBGs can be simultaneously interrogated by one single multichannel measurement device applying multiplexing technology. This provides a simple and low-cost method for dense monitoring.

The two most important schemes of multiplexing [19] are illustrated in Fig. 10.9. The first one is the time-division-multiplexing (TDM) technique, where each single sensor can clearly be identified by temporal gating the reflected signals. In that case the FBG sensors typically have an identical grating constant and low reflectivity. For the second approach—called the wavelength-division-multiplexing (WDM) technique—identification of each sensor is performed by processing Bragg gratings with different grating constants. Each single FBG sensor, which is deployed along the same optical fiber, must have a unique grating constant. Both techniques may be combined and, in addition, the number of available channels of the FBG measurement system can be extended by optical switches.

In the following only the WDM technique will be considered. For this method, a broadband light source such as a superluminescent light-emitting diode (SLED) or an amplified spontaneous emission (ASE) source is required [20]. The broadband light is coupled into the optical fiber and the spectral position of back-reflected
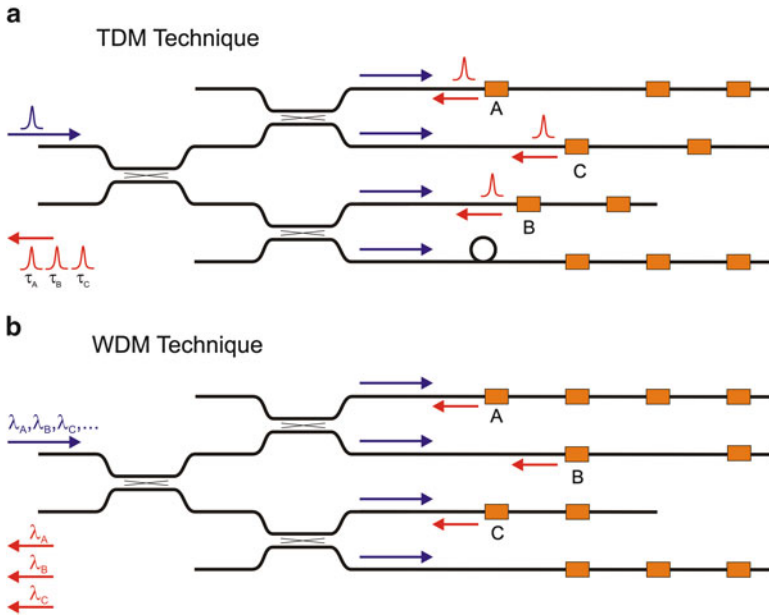
Fig. 10.9 Schematics for different kinds of fiber-optical multiplexing: (**a**) time-division-multiplexing (TDM) technique and (**b**) wavelength-division-multiplexing (WDM) technique. Both techniques may be combined and, in addition, the number of available channels of the FBG measurement system can be extended by using an optical switch

light related to the individual Bragg gratings is analyzed by a spectrometer. The spectral peak position of the reflected light gives information on the strain and/or temperature (refer to Eq. (10.2)—here n depends on temperature and Λ on mechanical strain). An optical switch allows sequential readout of several fiber strands. Most FBG measurement systems are optimized for wavelengths around 1,550 nm due to the wide availability of fiber-optical components used in the telecommunication industry [21].

Besides a pure strain and temperature sensor, the strain information of an ensemble of FBGs can also be used to calculate a 3D shape of the fiber if a special geometric arrangement of FBGs in the fiber is applied. Figure 10.10 shows the experimental setup for such a measurement device. The basic concept of fiber-optical 3D shape monitoring based on FBG sensor technology will be discussed in detail in the next section.
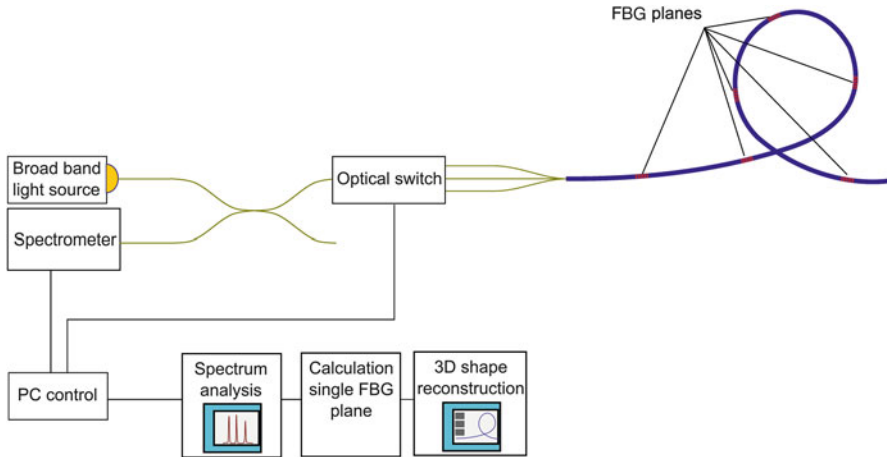
Fig. 10.10 Fiber Bragg grating readout system for 3D shape sensing

## 10.3.2 Fiber-Optical 3D Shape Sensing with FBGs

The 3D shape sensing approach applying FBG sensors is based on simple strain measurements that occur off-axis in a mechanical object during bending. The required spatial coordinates *x*, *y*, *z* equal to the three degrees of freedom, whereby only two degrees have to be determined for the shape sensing. The z-information is already fixed by the FBG sensor position along the optical fiber. Consequently, at least two independent grating sensors have to be applied in one spatial volume element. These two gratings form a so-called sensor plane which is orthogonal to the optical axis of the fiber. If temperature compensation has to be taken into account, a further FBG sensor has to be added. Therefore, a temperature-compensated fiber-optical 3D shape sensor consists of several sensor planes with at least three independent FBGs per plane. One possible arrangement is shown in Fig. 10.11. The individual FBG sensors are geometrically aligned in a 120° configuration.

With this setup the temperature-compensated *x*- and *y*-component of the bending process (ε_x and ε_y) can be stated as follows:

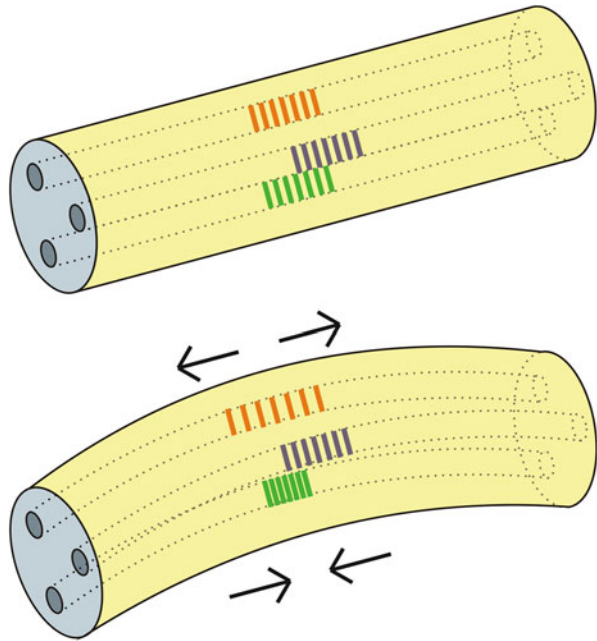$$\varepsilon_x = \frac{\varepsilon_2 - \varepsilon_3}{\sqrt{3}} \tag{10.9}$$

$$\varepsilon_y = \frac{2}{3}\left(\varepsilon_1 - \frac{1}{2}(\varepsilon_2 + \varepsilon_3)\right) \tag{10.10}$$

where ε_1, ε_2, and ε_3 are the strains measured by the corresponding FBG sensors in fiber core #1, #2, and #3, respectively (refer to Fig. 10.11b).
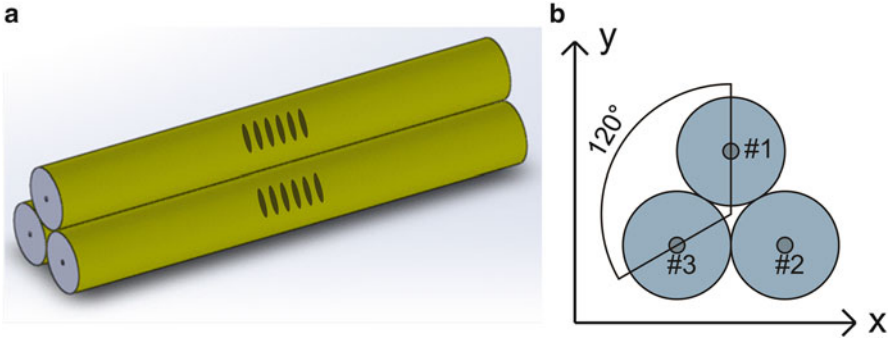
Fig. 10.11 (**a**) Combination of three single-core optical fibers. (**b**) 120° fiber configuration for shape monitoring

**Fig. 10.12** Schematic behavior of a fiber Bragg grating sensor plane during the bending process

Looking at Eqs. (10.9) and (10.10), one can see that a constant shift of the measured strain $\Delta\varepsilon = \Delta\varepsilon_1 = \Delta\varepsilon_2 = \Delta\varepsilon_3$ has no effect on ε_x and ε_y. The bending of the sensor elements leads to an expansion at one side and compression on the opposed side, respectively. This is illustrated in Fig. 10.12.

An alternative sensor configuration can be realized with four optical fibers arranged in a square, as illustrated in Fig. 10.13 [22]. With an additional strain ε_4 of sensor #4, the x- and y-component of the bending process will be reduced to

$$\varepsilon_x = \varepsilon_1 - \varepsilon_3 \tag{10.11}$$

Fig. 10.13 90° fiber
configuration of four fibers
with FBG sensors
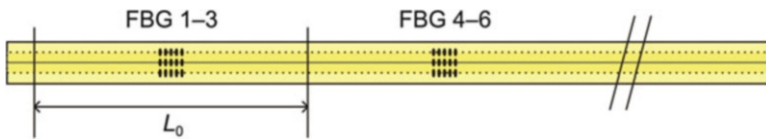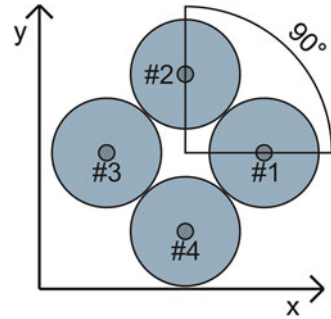
Fig. 10.14 Virtual segmentation of the bended structure in flexural elements, each one containing a single sensor plane

$$\varepsilon_y = \varepsilon_2 - \varepsilon_4 \tag{10.12}$$

10.3.3 Signal Evaluation and 3D Shape Reconstruction

The 3D shape is reconstructed by analyzing the strains ε_x and ε_y. Therefore elements with the length L_0, each containing one FBG sensor plane, can be defined (refer to Fig. 10.14). When bending the structure, the length of a neutral axis element L_0 remains constant, while the surface of the element is elongated or shortened. Caused by the 120° geometrical fiber configuration (refer to Fig. 10.12) all FBG sensors are located outside the neutral axis with the distance r and therefore are sensitive to bending-induced strain.
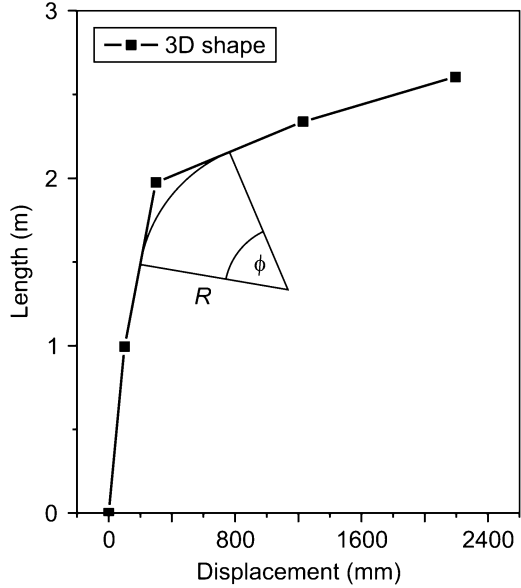
Assuming the element containing the Bragg gratings bends like an arc of a circle, the outer length L_{out} can be described using the sensor distance r and the central angle ϕ:

$$L_{out} = L_0 \pm \phi \cdot r \tag{10.13}$$

The strain with reference to the neutral axis can be expressed by

$$\varepsilon = \frac{L_{out} - L_0}{L_0} = \pm \frac{\phi \cdot r}{L_0} \tag{10.14}$$

Fig. 10.15 Two-dimensional projection of the 3D shape

Measuring the strain in *x*- and *y*-direction with FBG sensors, the central angles $\phi_{x,y}$ for the volume element can be calculated:

$$\phi_{x,y} = \pm \frac{\varepsilon_{x,y} \cdot L_0}{r} \tag{10.15}$$

With these angles also the radius of curvature *R* and azimuth angle φ can be determined:

$$R = \frac{L_0}{\sqrt{\phi_x^2 + \phi_y^2}} = \frac{r}{\sqrt{\varepsilon_x^2 + \varepsilon_y^2}} \tag{10.16}$$

$$\varphi = a \tan 2 \left(\phi_y, \phi_x \right) = a \tan 2 \left(\varepsilon_y, \varepsilon_x \right) \tag{10.17}$$

The most straightforward approach of 3D shape reconstruction combines the information for each volume element containing an FBG Sensor plane in sequence. Having *n* sensor planes distributed over the bending structure, there are also *n* elements. The start vector $\overrightarrow{r}_0$ from the base point [0 0 0] can be defined arbitrarily. Every vector $\overrightarrow{r_n}$ then can be determined by its previous vector $\overrightarrow{r_{n-1}}$ tilted over $\phi_{x,n}$ and $\phi_{y,n}$. Figure 10.15 illustrates a two-dimensional projection of the 3D shape, the radius of curvature *R*, and the central angle ϕ.

Another approach for the reconstruction of the 3D shape is based on the Frenet-Serret formulae. More details for this approach can be found in [23]. Results for 3D shape measurements given in this chapter are only based on the geometrical approach described above.
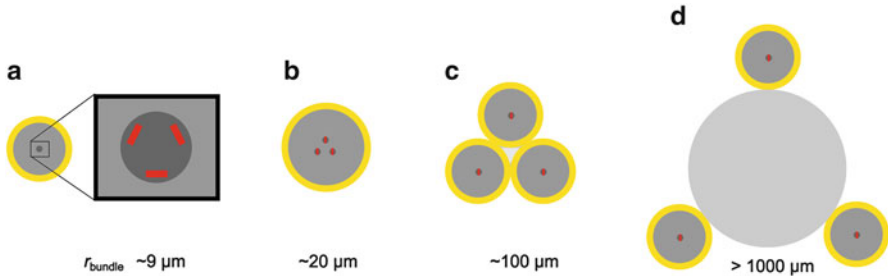
Fig. 10.16 Possible 120° geometrical configurations for fiber-optical 3D shape sensing applying FBG sensors

10.3.4 Resolution and Accuracy of 3D Shape Measurement

The requirements with respect to spatial resolution and measurement accuracy for an application of fiber-optical 3D shape sensing in the oil and gas industry, for example, the monitoring and long-term inspection of drill holes, are extremely different from that required for medical applications such as biopsy needles, endoscopes, or cardiac catheters. While the first application implies shapes and bending radii in the meter range on distances up to kilometers, a medical instrument requires resolution in the millimeter range with bending radii well below 50 mm for distances typically below 1 m.

A 3D shape calculated by the approach discussed above will only be reproducible if the three fiber cores are fixed to each other in the 120° geometrical configuration. Four different concepts can be considered. The first one is the superimposed writing of the FBG sensors into a single-mode fiber. The point-by-point inscription of FBGs with an ultrashort pulse laser allows the inscription of all three gratings within a single core with typical diameter of 9 μm. However, it was shown that the fidelity of such a fiber-optical shape sensor would be too small for most applications. The second possibility is the usage of a multicore fiber and has already been realized [24]. A larger diameter and, therefore, higher sensor fidelity can be achieved with a combination of three single-mode fibers forming a fiber bundle. This can be done by additional recoating or just by gluing these fibers to each other. For example, a viscous two-component adhesive can be used to create such a fiber bundle, however with the drawback in loss of mechanical flexibility. Even if the resulting diameter changes between two sensor planes, all three FBGs of one sensor plane will be fixed in their relative positions to each other. Therefore, the sensor can be calibrated with a correction factor for each sensor plane and optimal measurement and recalculation accuracy can be obtained. Fixing three separated fibers to a flexible carrier material is the fourth possibility (Fig. 10.16).

The mechanical stability of the fiber, the total spectral bandwidth of typical light sources, and the accuracy of the measurement system itself determine accuracy and dynamic range of the FBG sensor-based 3D shape sensor.
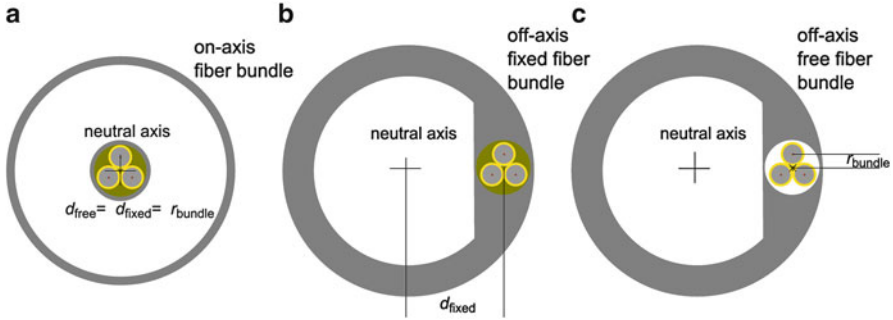
Fig. 10.17 (**a**) Typical on-axis integration of a shape sensing fiber bundle near the neutral bending center of the monitored device. (**b**) and (**c**) Possible off-axis integration. For small bending radii the sensor has to remain free (that means fixed only at one point) to avoid too high mechanical stress

In most applications, a shape sensing fiber bundle cannot be integrated in the center line of the mechanical device whose shape has to be monitored. Therefore, the fibers will be stretched and compressed depending on their distance d to the bending center (here the material remains neutral while bending) and the actual bending radius R. In the simplest case of a perfect circle, this leads to

$$\varepsilon = \frac{\Delta L}{L} = \frac{2\pi\,(R+d) - 2\pi R}{2\pi R} = \frac{d}{R} \tag{10.18}$$

For typical coated glass fibers the maximum possible elongation (ε) is about 2 %. Above that value the fiber can break and the FBG sensors will be destroyed. Therefore, the bending radius has to be larger than 50 times of the distance to the bending center. However, for some "off-axis" arrangements such as medical catheters (e.g., $d = 1.5$ mm $R = 25.0$ mm), it could be necessary to detect smaller bending radii. In that case, the shape sensing fiber has to be placed into the device (e.g., a catheter) without fixing it directly to the device. Then the sensors will not be elongated together with the surrounding material, but only by the shape itself, and the distance to the bending center becomes the radius of the fiber bundle r_{bundle} (refer to Fig. 10.17a).

An elongation of 2 % of the fiber equals a spectral shift of 24 nm for an FBG at 1,550 nm. On the other hand, a typical broadband light source (e.g., SLED) has a bandwidth of 50–70 nm and only within this spectral range Bragg grating signals can be analyzed. In order to achieve high accuracy for shape measurement, much more than one FBG sensor plane is necessary. Assuming twelve sensing planes and a spectral distance of 7 nm between single gratings a maximum elongation of 0.58 % for the fiber can be measured, if a mixing of different wavelengths has to be avoided. This should be preferred to simplify data analysis for shape reconstruction.

The sensor accuracy is limited by the spectral resolution of the FBG interrogator. For a typical spectrometer operating around 1,550 nm this can be estimated to be

Table 10.1 Range of detectable curvatures for fiber bundles with different diameters

| Fiber cladding diameter	125 µm	125 µm	80 µm	125 µm	125 µm
Bundle diameter (with polyimide coating)	9 µm (single core)	60 µm (multicore)	190 µm	280 µm	50 mm (three fibers)
r_{bundle}	~3 µm	~20 µm	70 µm	108 µm	25 mm
Max bending radius	0.46 m	3.08 m	10.8 m	16.6 m	3,846 m
Min bending radius (mechanical stability)	0.15 mm	1.0 mm	3.5 mm	5.4 mm	1.25 m
Min bending radius (12 sensors within 100 nm)	0.6 mm	5 mm	17.5 mm	27.0 mm	6.25 m

10 pm. Therefore, the minimum detectable fiber elongation is about 8.3×10^{-4} %. In order to measure bending radius and direction simultaneously it is necessary to analyze the relative differences in the wavelength shift signals of the three fibers. Assuming a circular curvature of the fiber bundle, the maximum bending radius is only depending on the bundle radius r_{bundle} and the minimum detectable elongation $\varepsilon_{\min}$:

$$r_{max} = \frac{r_{bundle}}{\varepsilon_{min}} \tag{10.19}$$

In Table 10.1 a summary of maximum and minimum bending radii for different fiber sensor configurations is given. It has to be considered that a bending radius <5 mm results in significant intensity losses of transmitted light in the fiber.

10.4 Medical Applications

As shown in the previous section, a wide dynamic range can be achieved by the use of different fiber configurations. This opens a wide field of possible applications for FBG-based shape sensing. For most small-scale applications like medical instruments, fiber bundles with diameters between 190 and 300 µm are a reasonable trade-off between accuracy and dynamic range of the shape sensor. In this section two applications of fiber-optical shape sensing will be discussed.
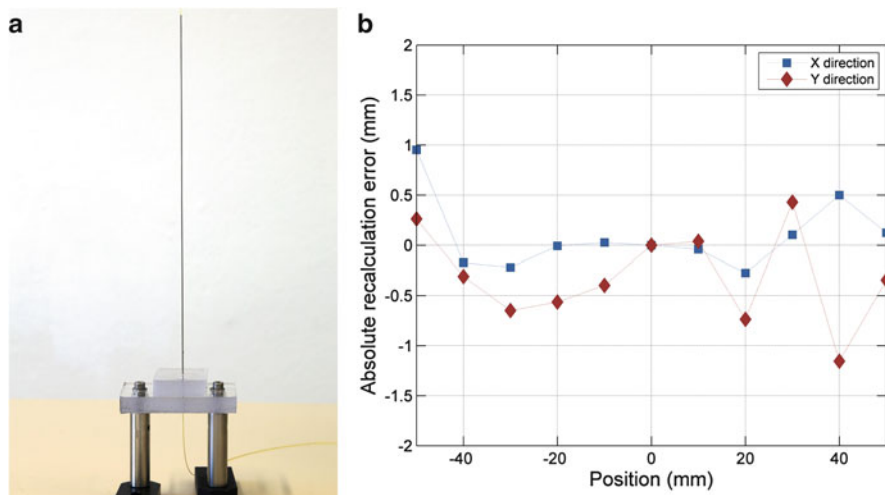
Fig. 10.18 (**a**) Capillary with four FBG sensor planes. (**b**) Accuracy of recalculated coordinates for the tip

10.4.1 Capillary Instruments

From the previous discussion it is obvious that best recalculation results of the 3D shape will be obtained if the device surrounding the FBG sensing fiber bends in a smooth and continuous way. Therefore a metal capillary with a diameter less than 5 mm will be a very good device for testing the spatial accuracy in 3D shape detection. Such device is similar to a biopsy needle.

Figure 10.18a shows a 35 cm long metal capillary (diameter 3 mm) with a 270 μm diameter fiber bundle consisting of four equidistant fiber FBG sensor planes. The tip of the capillary was moved by an xy-stage to defined positions within a field area of 10×10 cm^2. From the shape measurement the absolute position of the capillary tip can be calculated. The results of these measurements are then compared to the absolute and precisely known positions of the xy-stage. The results are shown in Fig. 10.18b. For *x*- and for *y*-directions an absolute error of less than ± 1 mm was found for the described geometrical configuration. This means that the position of the capillary tip can be navigated or tracked only by the fiber-optical shape sensor with an accuracy ± 1 mm. This offers new and very interesting possibilities for the navigation and tracking of medical instruments only by using a passive optical device such as an optical fiber. The major advantage is that this navigation device will not be influenced by electromagnetic fields that are always present in a clinical environment.
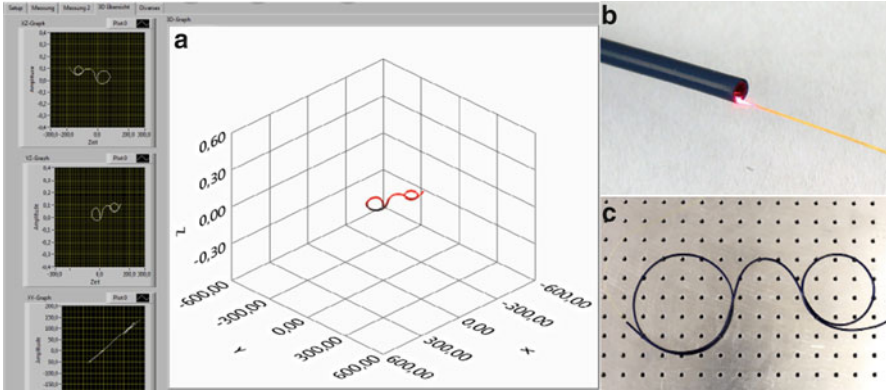
Fig. 10.19 (**a**) Screenshot of real-time recalculation of a catheter with eleven equidistant FBG sensor planes. (**b**) The fiber bundle is integrated into a 200 μm diameter tube which is part of the catheter. (**c**) The bended catheter

10.4.2 Medical Catheter

The real-time 3D shape measurement of a medical catheter will also offer the possibility for a new method of navigation of such an instrument which is not influenced by surrounding electromagnetic fields. Here the accurate shape detection of the catheter tip (most important is the last 10 cm of the catheter which is very flexible and which can be manipulated in all three directions in space by the operator) is compared to the blood system of a human body which is the pathway of the catheter, e.g., on its way to the heart. Comparing in real time the geometrical 3D shape of the catheter tip with the image of the blood system, which is the "map," the actual position of the catheter tip can be monitored. This allows navigation of the catheter just by measuring the 3D shape of the medical instrument. A first demonstration of this 3D shape measurement for a medical catheter is shown in Fig. 10.19.

In this case a fiber bundle consisting of three 80 μm diameter polyimide-coated optical fibers with a total diameter of 190 μm is used for the shape measurement. The 80 μm fibers have been used to guarantee most mechanical flexibility for the catheter and because the diameter of the tube where the fiber bundle has to be integrated inside the catheter has a limited diameter of about 200 μm, respectively. The total length of the catheter is 1.5 m, and the fiber bundle in total has 11 equidistant sensor planes, enabling 3D shape measurement across the whole length of the catheter.

One example of the shape measurement for the catheter is shown in Fig. 10.19. The catheter is bended into two circles with diameters of 6 cm and 4 cm, respectively. The complete recalculated shape from the strain measurements of the
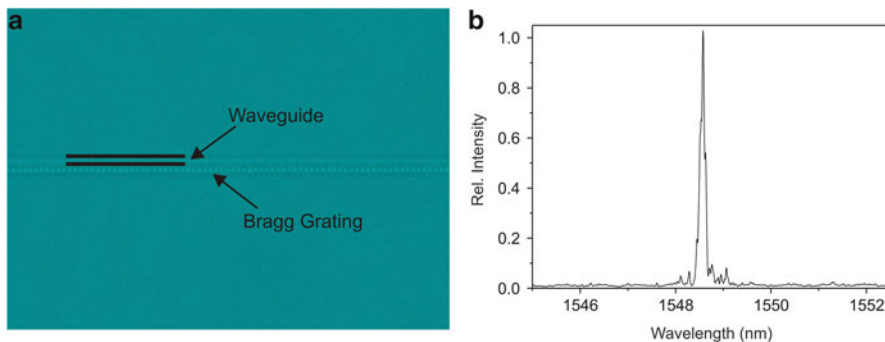
Fig. 10.20 (**a**) 3D point-by-point femtosecond laser processed waveguide and FBG in a glass plate. (**b**) Bragg reflection signal from the FBG shown in part (**a**) of the figure

integrated FBG sensors is shown in the screenshot. The shape of the catheter is reproduced very nicely. The left part of the screenshot also shows the projections of the 3D shape in the xz- and yz- as well as the xy-plane, which represents the linear stretched catheter. As a result, this demonstration shows that 3D shape measurement applying FBG sensor technology is an interesting new tool for navigation and tracking of medical instruments, such as catheters.

10.4.3 Single Fiber Shape Sensing

A completely different approach for 3D FBG shape sensors is possible by latest developments in another point-by-point femtosecond laser processing technique that allows direct writing of 3D waveguides into optical transparent materials (e.g., glass plates) and, in a second step, additional inscription of FBGs into waveguide. As shown in Fig. 10.20. From the microscope image the waveguide structure inside a glass plate can clearly be seen as well as the grating structure (a). In part (b) of the figure, the reflected Bragg signal of SLED light coupled into the waveguide is presented. This concept is transferred to the processing of waveguides and FBGs into the cladding material of a conventional single-mode optical fiber. By aligning the focus of the femtosecond laser into the cladding waveguides, FBGs can directly be processed by the point-by-point femtosecond laser technique. This enables us to develop completely new design for FBG-based shape sensors. One possible concept is shown in Fig. 10.21. FBGs are processed into the core of the fiber but also inside microscopic waveguides processed inside the cladding material of the fiber. Light from the fiber core is coupled into these waveguides via evanescent field effect; by aligning the distance between fiber core and additional cladding waveguide, the amount of coupled light can be controlled very accurately.
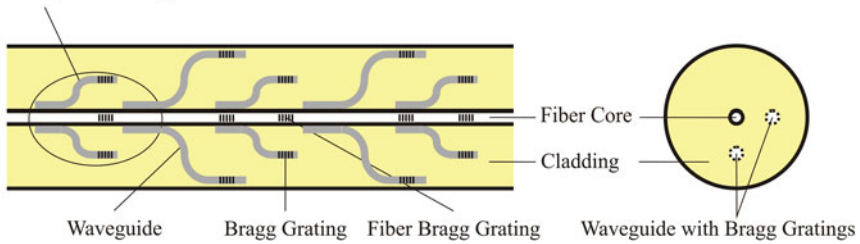
Fig. 10.21 Single-mode optical fiber for 3D shape sensing using laser-inscribed waveguides with integrated FBG sensor elements

Appling the 90° FBG sensor configuration as shown in Fig. 10.21, two waveguides with integrated Bragg gratings in the cladding allow the complete reconstruction of bending direction, radius, and, consequently, the 3D shape. One additional FBG in the fiber core is required for temperature and strain compensation. Compared to conventional 3-fiber arrangements or a multicore fiber, such a setup is easier to handle and much more comfortable to integrate into instruments (e.g., a medical catheter) where geometrical size and mechanical flexibility are important issues. In addition, the smooth surface of a pure fiber also helps significantly to avoid torsion effects that influence the accuracy of fiber-optical shape measurements. Another advantage of this approach is that no additional imaging optics are necessary as in the case of multicore fiber-based shape sensing systems. First experiments applying this very new concept are in progress at the Fraunhofer HHI and will be published very soon.

10.5 Conclusion

The point-by-point femtosecond laser processing technique of waveguides and FBGs in optical transparent materials opens a wide range of new possibilities in the design and fabrication of photonic sensor devices. In this context, 3D fiber-optical shape measurement based on FBG sensor technology will provide completely new tools for navigation and tracking of instruments used not only in medicine but also in industry, e.g., the exploration and maintenance of oil and gas wells. The femtosecond laser technique enables direct processing of FBGs in nearly all optical fibers but also especially in new fiber designs such as multicore fibers. Just by proper setting of the laser focus, the processing can be performed in a well-defined volume element of the material, and therefore 3D processing can easily be done. As an example, this allows addressing single cores of a multicore fiber for direct processing of FBGs. In addition, the femtosecond laser technique offers the possibility of also using a simple single-mode optical fiber for shape monitoring by direct processing of FBGs inside the cladding and fiber core material with the advantage of high mechanical

flexibility of the fiber and the use of conventional fiber connectors for coupling light into the fiber and analyzing the signals by a spectrometer. Besides this, the application of pulse trains (pulse shaping) for the waveguide and especially for the FBG processing in optical fibers results in significantly reduced pulse energies that are necessary for the processing. This results in much higher mechanical stability of the femtosecond laser processed Bragg gratings which will be important for measuring strong bending (e.g., application of this technique for navigation and tracking of cardiac catheters). In conclusion, this new fabrication method will give very interesting and innovative impacts for the design and processing of photonic sensor devices in the future.

References

1. K.O. Hill, Y. Fujii, D.C. Johnson, B.S. Kawasaki, Photosensitivity in optical fiber waveguides: application to reflection filter fabrication. Appl. Phys. Lett. **32**(10), 647 (1978)
2. G. Meltz, W.W. Morey, W.H. Glenn, Formation of Bragg gratings in optical fibers by a transverse holographic method. Opt. Lett. **14**(15), 823 (1989)
3. A. Martinez, M. Dubov, I. Khrushchev, I. Bennion, Direct writing of fibre Bragg gratings by femtosecond laser. Electron. Lett. **40**(19), 1170 (2004)
4. A. Martinez, I.Y. Khrushchev, I. Bennion, Thermal properties of fibre Bragg gratings inscribed point-by-point by infrared femtosecond laser. Electron. Lett. **41**, 176–178 (2005)
5. R.J. Roesthuis, M. Kemp, J.J. van den Dobbelsteen, S. Misra, Three-dimensional needle shape reconstruction using an array of fiber Bragg grating sensors (2013 accepted)
6. G.M.H. Flockhart, W.N. MacPherson, J.S. Barton, J.D.C. Jones, L. Zhang, I. Bennion, Two-axis bend measurement with Bragg gratings in multicore optical fiber. Opt. Lett. **28**(6), 387–389 (2003)
7. A. Othonos, Fiber Bragg gratings. Rev. Sci. Instrum. **68**(12), 4309–4341 (1997)
8. R. Kashyap, *Fiber Bragg Gratings*, 2nd edn. (Academic, Burlington, 2010)
9. J. Burgmeier, W. Schippers, N. Emde, P. Funken, W. Schade, Femtosecond laser-inscribed fiber Bragg gratings for strain monitoring in power cables of offshore wind turbines. Appl. Opt. **50**(13), 2011 (1868–1872)
10. J. Burgmeier, Erzeugung periodischer brechzahlmodulationen in glasfasern mit femtosekundenlaserpulsen und deren anwendung, Graduate thesis, Clausthal University of Technology (CUT), 2013
11. G.D. Marshall, R.J. Williams, N. Jovanovic, M.J. Steel, M.J. Withford, Point-by-point written fiber-Bragg gratings and their application in complex grating designs. Opt. Express **18**, 19844–19859 (2010)
12. L. Sudrie, A. Couairon, M. Franco, B. Lamouroux, B. Prade, S. Tzortzakis, A. Mysyrowicz, Femtosecond laser-induced damage and filamentary propagation in fused silica. Phys. Rev. Lett. **89**(18), 186601 (2002)
13. A. Othonos, K. Kalli, *Fiber Bragg Gratings: Fundamentals and Applications in Telecommunications and Sensing* (Artech House, Boston, 1999)
14. R.J. Williams, C. Voigtländer, G.D. Marshall, A. Tünnermann, S. Nolte, M.J. Steel, M.J. Withford, Point-by-point inscription of apodized fiber Bragg gratings. Opt. Lett. **36**(15), 2988–2990 (2011)

15. B. Malo, S. Theriault, D.C. Johnson, F. Bilodeau, J. Albert, K.O. Hill, Apodized in-fibre Bragg grating reflectors photo-imprinted using a phase mask. Electron. Lett. **31**(3), 223–225 (1995)
16. J. Canning, M.G. Sceats, π-phase-shifted periodic distributed structures in optical fibres by UV post-processing. Electron. Lett. **30**(16), 1344–1345 (1994)
17. R. Kashyap, P.F. McKee, D. Armes, UV written reflection grating structures in photosensitive optical fibres using phase-shifted phase masks. Electron. Lett. **30**(23), 1994 (1977–1978)
18. W.W. Morey, J.R. Dunphy, G. Meltz, Multiplexing fiber Bragg grating sensors. Distributed and multiplexed fiber optic sensors. Proc. SPIE **1586**, 216 (1992)
19. A.D. Kersey, M.A. Davis, H.J. Patrick, M. LeBlanc, K.P. Koo, C.G. Askins, M.A. Putnam, E.J. Friebele, Fiber grating sensors. J. Lightwave Technol. **15**(8), 1442–1463 (1997)
20. K.T.V. Grattan, T. Sun, Fiber optic sensor technology: an overview. Sensors Actuators A Phys. **82**(1), 40–61 (2000)
21. J. Koch, M. Angelmahr, W. Schade, Arrayed waveguide grating interrogator for fiber Bragg grating sensors: measurement and simulation. Appl. Opt. **51**(31), 7718–7723 (2012)
22. Y. Xinhua, Q. Jinwu, S. Linyong, Z. Yanan, Z. Zhen, An innovative 3D colonoscope shape sensing sensor based on FBG sensor array, in *International Conference on Information Acquisition*, Korea, 2007, pp. 227–232
23. J.P. Moore, M.D. Rogge, Shape sensing using multi-core fiber optic cable and parametric curve solutions. Opt. Express **20**(3), 2967–2973 (2012)
24. M.J. Gander, W.N. MacPherson, R. McBride, J.D.C. Jones, L. Zhang, I. Bennion, P.M. Blanchard, J.G. Burnett, A.H. Greenaway, Bend measurement using Bragg gratings in multicore fibre. Electron. Lett. **36**(2), 120–121 (2000)